Methane Emissions from the Munich Oktoberfest

Jia Chen[1,*]**, Florian Dietrich**[1,*]**, Hossein Maazallahi**[2,4]**, Andreas Forstmaier**[1]**, Dominik Winkler**[1]**, Magdalena E. G. Hofmann**[3]**, Hugo Denier van der Gon**[4]**, and Thomas Röckmann**[2]

[1]Environmental Sensing and Modeling, Technical University of Munich (TUM), Munich, Germany
[2]Institute for Marine and Atmospheric Research, Utrecht University, Utrecht, The Netherlands
[3]Picarro B.V., 's-Hertogenbosch, The Netherlands
[4]Climate, Air and Sustainability, TNO, Utrecht, The Netherlands
[*]Equal contribution

Correspondence: Jia Chen (jia.chen@tum.de), Florian Dietrich (flo.dietrich@tum.de)

Abstract. This study presents the first investigation of the methane (CH_4) emissions of a large festival. Munich Oktoberfest, the world's largest folk festival, is a potential source of CH_4 as a large amount of natural gas for cooking and heating is used.

In 2018 we measured the CH_4 emissions of Oktoberfest using in-situ measurements combined with a Gaussian plume dispersion model. Measurements were taken while walking and biking around the perimeter of the Oktoberfest premises (Theresienwiese) at different times of the day, during the week and at the weekend. The measurements showed enhancements of up to 100 ppb compared to background values and measurements after Oktoberfest. The average emission flux of Oktoberfest is determined as $(6.7 \pm 0.6)\,\mu\text{g}/(\text{m}^2\text{s})$. Additional analyses, including the daily emission cycle and comparisons between emissions and the number of visitors, suggest that CH_4 emissions of Oktoberfest are not due solely to the human biogenic emissions. Instead, fossil fuel CH_4 emissions, such as incomplete combustion or loss in the gas appliances, appear to be the major contributors to Oktoberfest emissions.

Our results can help to develop CH_4 reduction policies and measures to reduce emissions at festivals and other major events in cities. Furthermore, events with a limited duration have not yet been included in the state-of-the-art emission inventories, such as TNO-MACC, EDGAR or IER. Our investigations show that these emissions are not negligible. Therefore, these events should be included in future emission inventories.

1 Introduction

Climate change is a global problem that is having a profound impact on living conditions and human societies. The present global warming is very likely due to strong anthropogenic greenhouse gas (GHG) emissions. The Paris Agreement establishes an international effort to limit the temperature increase to well below $2\,°\text{C}$ above pre-industrial levels. A "global stocktake" will revisit emission reduction goals every five years starting in 2023. The EU aims to cut its GHG emissions by $40\,\%$ by 2030 and by $80\,\%$ to $95\,\%$ by 2050, compared to the 1990 level. The German climate action plan (Klimaschutzplan 2050) contains similar goals, i.e. to cut at least $55\,\%$ of German GHG emissions by 2030 and at least $80\,\%$ by 2050.

Methane (CH_4) is the second-most prevalent GHG emitted by human activities (Allen et al. (2018); Etminan et al. (2016); Myhre et al. (2013)). It is estimated to have a global warming potential (GWP) that is 28 to 34 times larger than that of CO_2 over the 100-year-horizon (IPCC (2013)). According to Etminan et al. (2016) the GWP is even $14\,\%$ higher than the reported values in IPCC. CH_4 has been responsible for around $20\,\%$ of the global warming by anthropogenic greenhouse gases since 1750 (Nisbet et al. (2014); Kirschke et al. (2013)). Current atmospheric CH_4 concentrations are 2.5 times as high as the pre-industrial levels, and since the industrial revolution its concentration growth has been 3 times faster than that of CO_2. After experiencing a nearly constant CH_4 concentration (total amount of CH_4 in the atmosphere) from 1999-2006, CH_4 concentrations have started to increase again (Saunois et al. (2016); Nisbet et al. (2014)). The reasons for the renewed growth are not fully

understood; fossil fuel methane emissions are largely underestimated (Schwietzke et al. (2016)) and could play a major role in it (Hausmann et al. (2016); Worden et al. (2017)). Natural gas is a growing source of energy, but its unwanted release into the atmosphere is a significant component of anthropogenic CH_4 emissions (Schwietzke et al. (2014); McKain et al. (2015)), and its reduction may be essential for attaining the goal of the Paris agreement.

Therefore, recent investigations have concentrated on detecting and quantifying CH_4 emissions from city gas pipelines, power plants as well as other gas and oil facilities using various methods. Phillips et al. (2013) mapped CH_4 leaks across all urban roads in the city of Boston using a cavity ring-down mobile analyzer. They identified 3,356 leaks with concentrations exceeding up to 15 times the global background level, and used their isotopic signatures to show that the leaks are associated with natural gas. Roscioli et al. (2015) described a method using dual-tracer flux ratio measurements complemented by on-site observations to determine CH_4 emissions from natural gas gathering facilities and processing plants. Toja-Silva et al. (2017) used differential column measurements (Chen et al. (2016)) and a computational fluid dynamics (CFD) model to quantify emissions from a natural-gas-based power plant in Munich. Atherton et al. (2017) conducted mobile surveys of CH_4 emissions from oil and gas infrastructures in northeastern British Columbia, Canada and used the CO_2/CH_4 ratios to identify these emissions. Weller et al. (2018) evaluated the ability of mobile survey methodology (von Fischer et al. (2017)) to find natural gas leaks and quantified their emissions. Yacovitch et al. (2015) measured CH_4 and ethane (C_2H_6) concentrations downwind of natural gas facilities in the Barnett shale region using a mobile laboratory. A couple of years later, Yacovitch et al. (2018) investigated the Groningen natural gas field, one of Europe's major gas fields, using their mobile laboratory in combination with airborne measurements. Luther et al. (2019) deployed a mobile sun-viewing Fourier transform spectrometer to quantify CH_4 emissions from hard coal mines. Other studies laid a special focus on city and regional emissions of fossil fuel CH_4. McKain et al. (2015) determined natural gas emission rates for the Boston urban area using a network of in-situ measurements of CH_4 and C_2H_6 and a high resolution modeling framework. Lamb et al. (2016) quantified the total CH_4 emissions from Indianapolis using the aircraft mass balance method and inverse modeling of tower observations, and distinguished its fossil fuel component using C_2H_6/CH_4 tower data. Wunch et al. (2016) used total column measurements of CH_4 and C_2H_6 recorded since the late 1980s to quantify the loss of natural gas within California's South Coast Air Basin. Most recently, Plant et al. (2019) reported aircraft observations of CH_4, CO_2, C_2H_6, and carbon monoxide (CO) of six old and leak-prone major cities along the East Coast of the United States. They found emissions attributed to natural gas are about a factor of 10 larger than the values provided by the EPA inventory.

Large folk festivals are also likely sources of anthropogenic emissions of air pollutants, such as nitrogen oxides (NO_x), CO, particulate matter (PM2.5, PM10), Sulfur dioxide (SO_2), etc. Huang et al. (2012) investigated the impact of human activity on air quality before, during, and after the Chinese Spring Festival 2009, the most important festival in China. They used potential source contribution function analysis to illustrate the possible source for air pollutants in Shanghai. Shi et al. (2014) measured concentrations of particulate matters and polycyclic aromatic hydrocarbons (PAHs) during the Chinese New Year's Festival 2013 and estimated the source attributions from cooking, vehicle, and biomass and coal combustion. Kuo et al. (2006) investigated PAH and lead emissions from cooking during the Chinese mid-autumn festival. Nishanth et al. (2012) reported elevated concentrations of various air pollutants such as ozone (O_3), NO_x, and PM10 after the traditional Vishu festival in South India. Nevertheless, up to now, festivals have not been considered a significant source of CH_4 emissions and accordingly, to the best of our knowledge, CH_4 emissions from large festivals have not yet been studied.

Oktoberfest, the world's largest folk festival with over 6 million visitors annually, is held in Munich. In 2018, during the 16 days of Oktoberfest, approximately 8-million liters of beer were consumed. For cleaning, dish washing, toilet flushing, etc., about 100-million liters of water were needed. The use of energy added up to 2.9 million kWh of electricity and $200,937\,\mathrm{m}^3$ of natural gas, 79 % of which is used for cooking and 21 % for heating (München (2018a)).

The measurements during our 2017 Munich city campaign indicated Oktoberfest as a possible source for CH_4 for the first time (Chen et al. (2018)). For a better source attribution and a quantitative emission assessment, we have investigated the CH_4 emissions from Oktoberfest 2018 by carrying out mobile in-situ measurements and incorporating a Gaussian plume dispersion model. These measurements and modeling approaches are described in section 2. The results of these investigations show that Oktoberfest is an anthropogenic source of CH_4 that has not been accounted for until now. We have compared the determined total emission flux with bottom-up estimates of biogenic emissions from human, and also present the daily cycle of the emissions. In addition, the week and weekend variations are shown. From these findings we can draw conclusions about the origins of the Oktoberfest CH_4 emissions, which are presented in section 3.

2 Method

We conducted a mobile survey around the perimeter of Oktoberfest to obtain the CH_4 concentration values around the festival area (Theresienwiese) and incorporated a Gaussian

plume model consisting of 16 different point sources to determine the CH_4 emission strength.

2.1 Measurement approach and instrumentation

The measurements include both CH_4 and wind measure-
ments. The sensors and the way they are used are described
in the following.

2.1.1 Concentration measurements

Mobile in-situ measurements were conducted to quantify
CH_4 enhancements. To this end, two portable Picarro Gas-
Scouters G4302 for measuring CH_4 and C_2H_6 were used.
The sensor is based on the cavity ring-down measurement
principle (O'Keefe and Deacon (1988)), using a laser as a
light source and a high-finesse optical cavity for measuring
gas concentrations with high precision, which is $3\,ppb$ for
CH_4 mode with $1\,s$ integration time (Picarro (2017)). We ap-
plied a moving-average filter with a window size of $10\,s$ and
a step size of $5\,s$ to the $1\,s$ raw measurements. Since the data
are averaged over $10\,s$, the precision is improved to $1\,ppb$.
To distinguish between fossil-fuel related and biogenic emis-
sions, the instrument can be switched to CH_4/C_2H_6 mode
and measure C_2H_6 with a precision of $10\,ppb$ for an integra-
tion time of $1\,s$.

Since we were not allowed to enter the festival area due to
safety concerns, the measurements were carried out by walk-
ing and biking many times around the perimeter of Okto-
berfest next to the security fences, wearing the analyzer as
a backpack. The measurements were taken on several days
during and after the time of the festival to compare the dif-
ferences in emission strength and distribution. Additionally,
to observe the hourly dependency of the emissions, the mea-
surements were distributed over the course of the day. In the
end, we covered the period between 8:00 a.m. and 7:00 p.m.
(local time) hourly.

For the study, two identical GasScouters G4302 were de-
ployed. One instrument was provided by TNO and the other
by Picarro Inc. The former was used in the first week while
the latter was used in the second week of Oktoberfest as well
as the time after the festival. Although the measurement ap-
proach is based on determining the enhancements and not
on comparing absolute concentration values, the two instru-
ments were calibrated at the beginning of the campaign.

2.1.2 Wind measurements

In addition to the gas concentrations, wind measurements are
vital for estimating the emissions of Oktoberfest using atmo-
spheric models. To this end, a 2D ultrasonic wind sensor (Gill
WindObserver II) was placed on a roof close by (48.148° N,
11.573° E, 24 m agl.). These wind measurements were uti-
lized for the emission estimates.

To assess the uncertainty of the wind measurements, we
compared these measurements with the values reported by
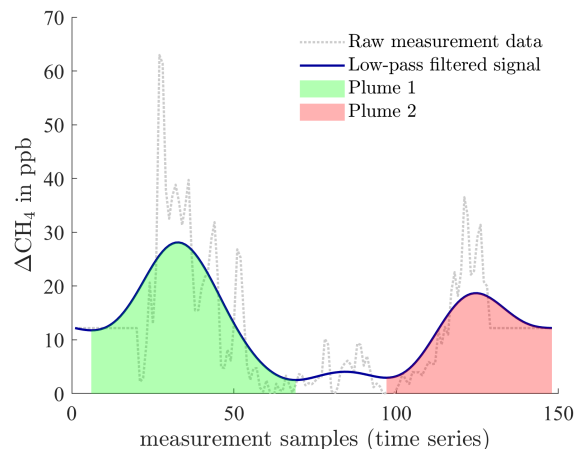
Figure 1. The pre-processed measurement signal (dotted line, mov-
ing average with window size $10\,s$ and step size $5\,s$) is shown along
with a low pass filtered version (blue line), which is used to obtain
the single plumes (green and red area). The signal in the center is
not detected as a plume, as the enhancement is not high enough. The
round shown was recorded by bike and took $750\,s$ ($12.5\,minutes$).

an official station of Germany's National Meteorological
Service (Deutscher Wetterdienst, DWD). The DWD station
(48.163° N, 11.543° E, 28.5 m agl.) is located about $2.8\,km$
away. As this distance is about the radius of the Munich inner
city, we assumed that the difference between the two stations
is representative for the uncertainty of two arbitrary measure-
ment points in the downtown area, which is also home to Ok-
toberfest.

2.2 Modeling approach

To quantify the emissions of Oktoberfest, we used the mea-
sured concentration values as input for an atmospheric trans-
port model.

2.2.1 Selection Algorithm

For our modeling approach, the plumes of individual surveys
(hereafter referred to as "rounds") around the Theresienwiese
were evaluated. In total, we completed 94 rounds (69 dur-
ing and 25 after Oktoberfest). For every round the individ-
ual plumes were determined by analyzing a low-pass filtered
version of the measurement time series. A Kaiser window
(Kaiser and Schafer (1980)) was utilized for the low-pass fil-
tering.

Once the signal was filtered, a signal section between two
adjacent minima was defined as a plume signal if it had an en-
hancement of more than $5\,ppb$. We chose this threshold to be
equal to the combined uncertainty of the instrument ($3\,ppb$)
and background ($4\,ppb$) (cf. section 2.2.6). This process is
illustrated in Figure 1.
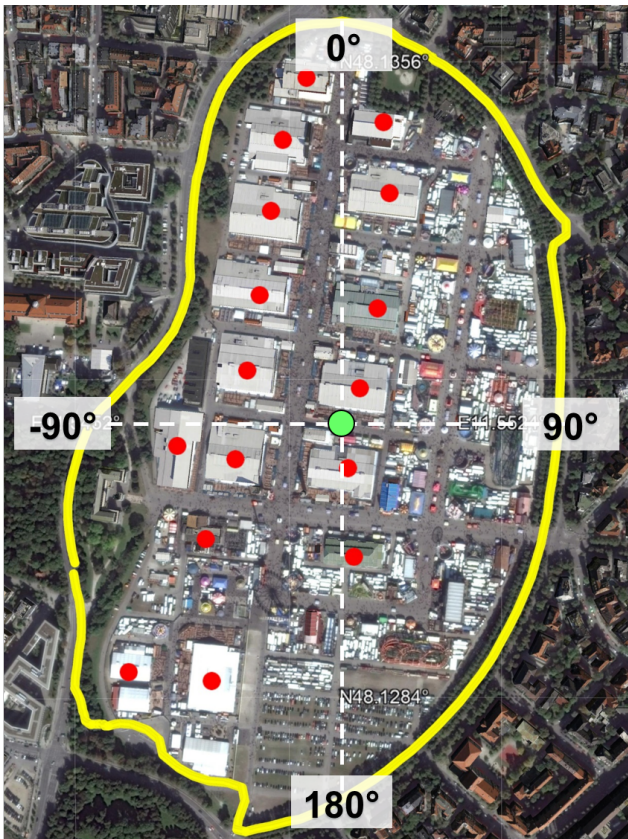
Figure 2. Standard route around Oktoberfest (yellow) including the locations of the 16 tents (red) and the center point (green). Map data: © Google, DigitalGlobe

When the initial plume selection phase was completed, the identified plumes were further analyzed. As the path of a measurement around the Oktoberfest premises was predefined by the security fence, the location of each point on that route can be converted into a fixed angle, which simplifies the comparison between the measurements and the model. For that purpose, a center point of the Theresienwiese was defined (cf. green dot in Figure 2, 48.1315° N, 11.5496° E). With the help of this point, an angle was assigned to all measurement and model values. This angle was defined similarly to the wind angles, meaning that 0° is in the north and 90° is in the east.

In order to decide whether a measured plume is attributable to emissions from Oktoberfest, a forward model uses the measured wind direction (with uncertainty) to calculate at which angles a plume from Oktoberfest should occur. As can be seen in Figure 3, only plume 1 was selected because the angle range of this plume (green) largely overlaps with the accepted angle range (grey) computed by the forward model of this plume. In contrast, plume 2 (red) has no overlap with the range computed by the forward model; hence, plume 2 was discarded.
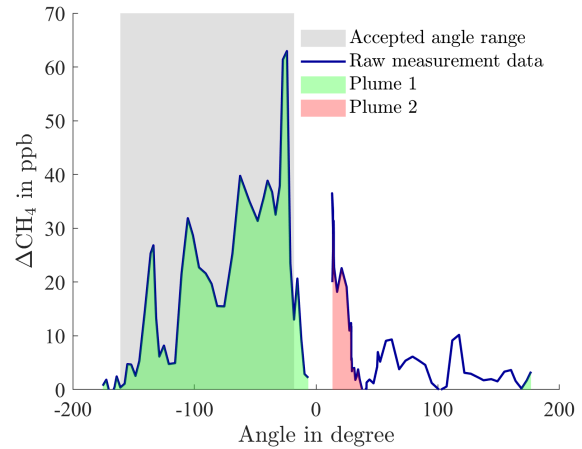
Figure 3. Measurement signal mapped onto the standard route with the angle on the abscissa. Two detected plumes and the accepted angle range computed by the forward model are highlighted. Plume 2 has no overlap with the accepted range and is therefore discarded.

Additionally, the standard deviation of the wind direction over the time the plume was recorded is taken into account. If the standard deviation is higher than 24°, the plume is not considered, as our approach requires stable wind conditions. Those 24° represent the measurement uncertainty in the wind direction (cf. 2.2.6) and are therefore well suited as a lower limit for filtering out too variable wind conditions.

The selection algorithm described above is visually summarized in Figure 4:
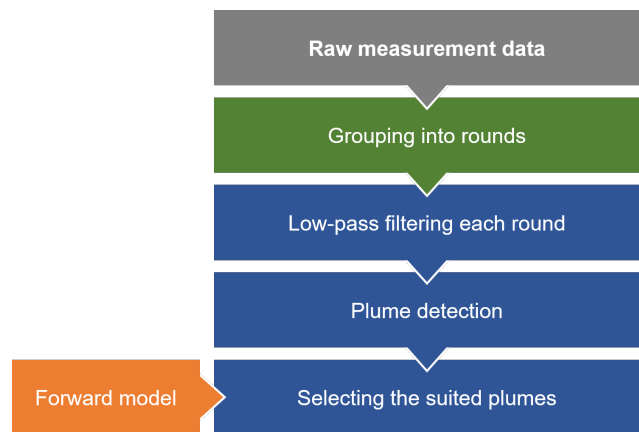
Figure 4. Flowchart visualizing the main steps performed on the raw measurement data in order to obtain an emission estimate.

2.2.2 Baseline determination

As one measurement round can take up to one hour (when walking), the atmospheric conditions can vary during that time period, which will result in a changing background concentration. Therefore, the baseline for determining the con-
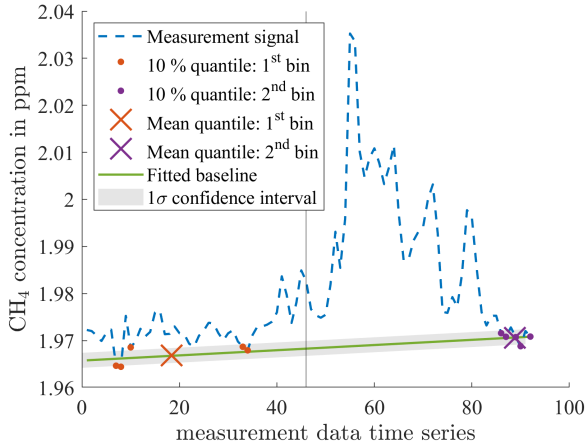
Figure 5. Baseline determination by dividing the measurement signal (blue) into two halves. Afterwards, a line (green) is fitted through the mean values of the 10 % lowest concentration points of each half. The grey shaded area denotes the 1σ uncertainty range of the background line.

centration enhancements cannot be calculated solely using a constant value.

In our approach, we assume that the baseline during one round is either rising or falling and that there is a linear behaviour. Such a straight line is clearly defined by two points. For that reason, the time series for each round was divided into two equally sized bins (first and second half). For each half, we determined the lowest 10 % quantile. Afterwards, the mean values of the 10 % smallest concentration values of each bin were used to define one straight line, which was used as the background for that specific round (cf. Figure 5). The uncertainty of that baseline was determined using the CH_4 concentration deviations of the 10 % smallest values from the baseline.

2.2.3 Gaussian plume model

The framework of our modelling approach is based on a Gaussian plume model described in Pasquill (1966, 1969, 1979); Gifford (1976); Briggs (1973); Hanna et al. (1982), and widely used to access local source emissions (Bovensmann et al. (2010); Yacovitch et al. (2015); Atherton et al. (2017); Nassar et al. (2017); Kiemle et al. (2017)). It is a steady-state model that simulates the diffusion and the transport of emitted trace gases from a point source. The gas disperses such that its concentration distributions fit well to Gaussian curves in vertical and horizontal directions.

For a point source emitting continuously with strength Q (unit: $mol\,s^{-1}$) at effective height H above the ground and uniform wind speed, the expression for the time-averaged concentration $<c(x,y,z)>$ (unit: $mol\,m^{-3}$) is given by the

formula below:

$$< c(x,y,z) >= \frac{Q}{2\,\pi\,\overline{u}\,\sigma_y(x)\,\sigma_z(x)} \exp\left(-\frac{y^2}{2\,\sigma_y(x)^2}\right) \times$$
$$\times \left(\exp\left(-\frac{(z-H)^2}{2\,\sigma_z(x)^2}\right) + \exp\left(-\frac{(z+H)^2}{2\,\sigma_z(x)^2}\right)\right) \quad (1)$$

with x, y and z describing the downwind distance, horizontal/cross-wind distance to the x axis, and the height above the ground, respectively. $\overline{u}$ is the time-averaged wind speed, $\sigma_y(x)$ is the standard deviation of the concentration in the cross-wind direction and $\sigma_z(x)$ is the standard deviation of the concentration in the vertical direction. These dispersion coefficients describe the spreading of a plume increasing with the downwind distance from the source x.

To determine the dependency of σ_y and σ_z on x, diffusion experiments were carried out (Haugen et al. 1958), which resulted in Pasquill's curves (Pasquill (1979); Gifford (1976)). Smith (1968) worked out an analytic power-law formula for the relationship between σ_y, σ_z and x. Briggs (1973) combined the aforementioned curves and used theoretical concepts to produce the widely used formulas given in Hanna et al. (1982).

During the measurement periods, the surface wind was lower than $4\,m\,s^{-1}$ and the insolation was strong to moderate. Therefore, stability class A or B was chosen according to the Pasquill turbulence types (Gifford (1976)).

Based on Briggs' recommendations for urban conditions (Briggs (1973); Hanna et al. (1982)), the relationships between the dispersion parameters and the downwind distance are described as:

$$\sigma_y(x) = 0.32\,x\,(1 + 0.0004\,x)^{-1/2}, \quad (2)$$

$$\sigma_z(x) = 0.24\,x\,(1 + 0.001\,x)^{1/2}. \quad (3)$$

These relationships were used in our study.

2.2.4 Multiple Gaussian plume model

The concentration measurements using the backpack instrument were performed close to the festival area ($< 500\,m$), which is why the emissions of Oktoberfest cannot be seen as a single point source. Accordingly, multiple point sources were used, which were modelled using Gaussian plumes before they were superimposed. The spatially superimposed plumes were detected as a continuous plume signal in our measurement. Later on, these plume signals were utilized for the emission assessment.

Since the emission sources of Oktoberfest were unknown, the locations with the highest density of visitors and with the highest energy consumption were chosen as the main sources for the model. Those locations are represented by the 16 biggest beer tents (> 1,000 seats) on the festival premises (cf. red dots in Figure 2). To achieve a good correlation between

the model and reality, these 16 tents were not treated equally in the final model. Instead, they were linearly weighted according to their maximum number of visitors. Therefore, the largest tent (about 8,500 visitors) has, in the end, a greater than eight times higher influence on the total emission number than the smallest tent (about 1,000 visitors).

2.2.5   Forward modelling approach

The multiple Gaussian plume model was used in a forward approach to compare the measured and modeled concentration signals with each other. For that, a predefined route around Oktoberfest was used (cf. yellow route in Figure 2) to determine the concentrations for each angle.

The actual shape of the concentration vs. angle graph $c(\alpha)$ for every selected plume i is considered for the determination of the emission number of Oktoberfest $E_{\mathrm{Okt},i}$ (cf. Figure 6, blue curve). The optimization procedure can be expressed mathematically as follows:

$$E_{\mathrm{Okt},i} = \underset{E_i}{\arg\min} \int_0^{360} |c(\alpha) - M(E_i, \alpha)| \, \mathrm{d}\alpha, \tag{4}$$

where M represents the model. The emission number E_{i} was varied until the areas underneath the modelled and measured curves are the same, and thus the sum of the absolute difference between the model and measurement is minimized.

Specifically, we computed the forward model using the averaged wind information at this time and a prior emission number E_{prior} of $3\,\mu\mathrm{g\,s^{-1}\,m^{-2}}$ and compared it with the measurement curve. If the shapes look similar (high cross-correlation coefficient), a scaling factor is applied to the prior emission number and varied until the forward model matches the measurements. This procedure is illustrated for one exemplary plume signal in Figure 6. There, the prior modelled concentrations (orange) are smaller than the measured concentrations (blue). Therefore, the model has to be multiplied with a scaling factor until the areas underneath the modelled and measured curve are the same (yellow). By multiplying the scaling factor $k_{\mathrm{scaling},i}$ with the E_{prior}, the emission number of Oktoberfest $E_{\mathrm{Oktoberfest},i}$ for every plume signal i can be determined as:

$$E_{\mathrm{Okt},i} = E_{\mathrm{prior}} \cdot k_{\mathrm{scaling},i}. \tag{5}$$

2.2.6   Uncertainty assessment

To determine the uncertainty of the final emission numbers, we considered the uncertainties of our input parameters. These include uncertainties in the wind and concentration measurements as well as uncertainties in the determined baseline. These input parameters were each modelled as a Gaussian distribution. Afterwards, the emission number was determined by running our modeling approach 1,000 times
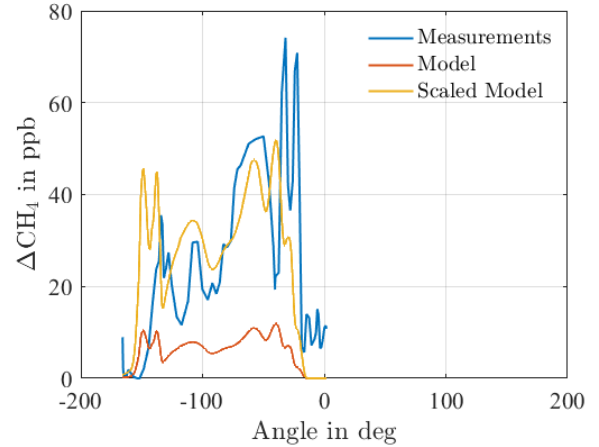
Figure 6. Raw measurement curve (blue) with the a priori forward model (orange) and the scaled forward model (yellow).

using those four parameters (wind speed, wind direction, measured CH$_4$ concentration, background concentration) as input. In each run, slightly different input values were chosen randomly and independent from each other out of those four distributions.

The concentration measurement uncertainty is indicated by the manufacturer Picarro to be about $1\,\mathrm{ppb}$ for an integration time of $10\,\mathrm{s}$. This value was used as the standard deviation of the modelled input distribution.

For the wind speed and direction, the instrument uncertainty as well as the spatial variations of the winds were taken into account. For that reason, the uncertainty of the wind measurements was determined by comparing two surface measurement stations within the inner city of Munich (cf. section 2.1.2). We determined the differences in wind speed and direction throughout September and October 2018. The differences are representative of the heterogeneity of the wind within the inner city of Munich and, therefore, represent an upper bound for the uncertainty of the wind within the Oktoberfest premises. The comparison of both the wind speed and direction resulted in Gaussian shaped distributions with mean values each around zero. The standard deviations of the differences between the reported wind directions and speeds of the two stations are $24°$ and $0.5\,\mathrm{m\,s^{-1}}$ throughout September and October 2018.

The baseline approach described in section 2.2.2 introduces a further error which has to be considered as well. Therefore, the background concentrations were modelled as a Gaussian distribution where its standard deviation was calculated from the CH$_4$ concentration deviations between the smallest $10\,\%$ values of each bin and the baseline shown in Figure 5.

The parameters used for the uncertainty assessment are summarized in Table 1.

Table 1. Mean and standard deviation of the input parameters for the CH_4 plume signal i

Type	Mean	Standard deviation
Wind speed	$v_{\mathrm{wind,meas},i}$	$0.5\,\mathrm{m\,s}^{-1}$
Wind direction	$\alpha_{\mathrm{wind,meas},i}$	$24°$
Instrumentation	$c_{\mathrm{meas},i}$	$1\,\mathrm{ppb}$
Background	$c_{\mathrm{backgnd},i}(t)$	$\sigma_{10\%\ \mathrm{quantile},i}$

3 Results and discussion

3.1 Concentration mapping

The measured CH_4 concentrations were plotted for each round on a map of the Oktoberfest premises to show that there is a clear correlation between the wind directions and the enhancements. As the variations of the boundary layer height should not be taken into account, these plots do not show the absolute concentration values but just the enhancements above the determined background concentrations (cf. section 2.2.2). Two such plots for two different wind directions are shown in Figure 7. In addition to the concentration enhancements and the wind direction, the 16 emission sources are shown as black dots on top of each tent. The Gaussian plumes themselves are also represented. These two plots reveal that the highest concentration enhancements can be observed downwind of the Oktoberfest premises.

3.2 Emission number

The average emission number of the Oktoberfest 2018 $E_{\mathrm{Okt,\ avg}}$ is determined by averaging the emission numbers of the N plume signals $E_{\mathrm{Okt,i}}$ during the complete Oktoberfest time period (including the weekdays and weekends), accordingly:

$$E_{\mathrm{Okt,\ avg}} = \frac{1}{N}\sum_{i=1}^{N} E_{\mathrm{Okt,i}}. \tag{6}$$

To make the final emission number more robust and to determine an uncertainty, the basic approach of Eq. 6 was improved. Instead of just using the actual measured data, an uncertainty range was applied to the four main input parameters, each using Gaussian distributions (cf. section 2.2.6).

For every plume signal i, 1,000 samples of randomly chosen input datasets from the aforementioned normal distributions of the input parameters were used to determine 1,000 slightly different emission numbers $E_{\mathrm{Okt,\ i,\ k}}$. Using Eq. 6, an average emission number for each realization $E_{\mathrm{Okt,\ avg,\ k}}$ was calculated:

$$E_{\mathrm{Okt,\ avg,\ k}} = \frac{1}{N}\sum_{i=1}^{N} E_{\mathrm{Okt,i,\ k}}. \tag{7}$$
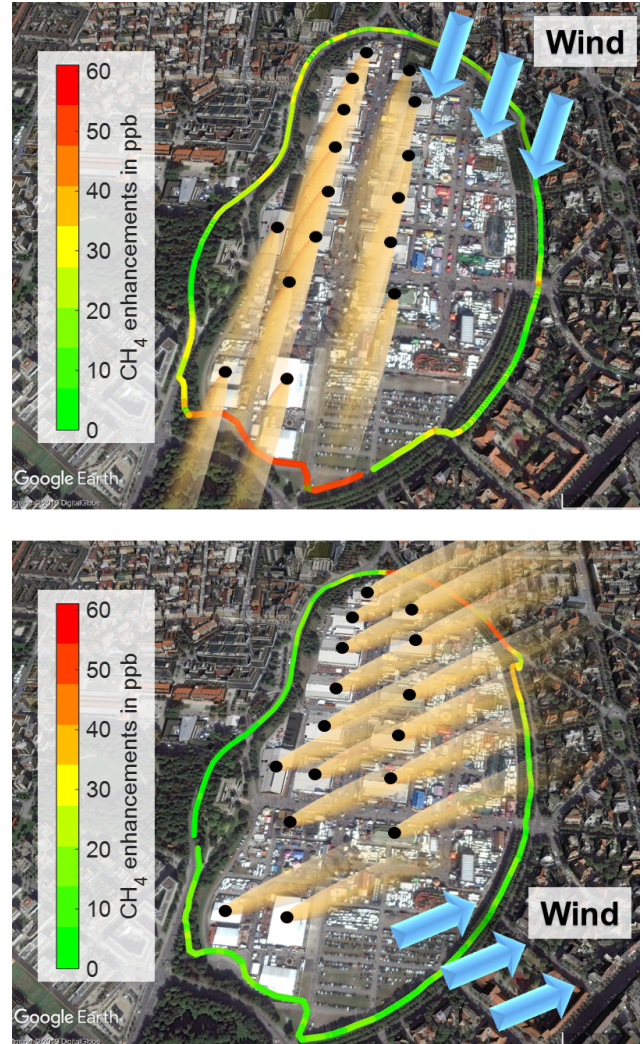
Figure 7. CH_4 concentrations of two measurement rounds including the influence of the 16 Gaussian plumes from the tents (black dots).

Wind direction: upper panel $20°$, lower panel $-110°$. Map data: © Google, DigitalGlobe

The average emission number including an uncertainty assessment can be obtained by determining the mean μ_{Okt} and standard deviation σ_{Okt} of those 1,000 realizations:

$$\mu_{\text{Okt}} = \frac{1}{1000} \sum\nolimits_{k=1}^{1000} E_{\text{Okt,avg, k}}, \tag{8}$$

$$\sigma_{\text{Okt}} = \sqrt{\frac{\sum_{k=1}^{1000} (E_{\text{Okt,avg, k}} - \mu_{\text{Okt}})^2}{999}}. \tag{9}$$

The result for the total emission number of Oktoberfest 2018 is shown in Figure 8 and has a value of

$$E_{\text{Okt,total}} = \mu_{\text{Okt}} \pm \sigma_{\text{Okt}} = (6.7 \pm 0.6)\,\mu\text{g}/(\text{m}^2\text{s}). \tag{10}$$

To verify whether those emissions were caused by the Oktoberfest, Figure 8 also shows the emissions determined for the time after Oktoberfest (from October 8th through October 25th). This number ($(1.1 \pm 0.3)\,\mu\text{g}/(\text{m}^2\text{s})$) is significantly smaller than the one during Oktoberfest but still not zero. It indicates that the emissions are caused by Oktoberfest, and the disassembling of all the facilities, which takes several weeks, still produces emissions after Oktoberfest.

After grouping the emission numbers into the two categories, weekday (in total 59 valid plumes) and weekend (26 valid plumes), two separated distributions are visible in Figure 9. The average emission for the weekend ($(8.5 \pm 0.7)\,\mu\text{g}/(\text{m}^2\text{s})$) is higher than the averaged emission for the weekdays ($(4.6 \pm 0.9)\,\mu\text{g}/(\text{m}^2\text{s})$), almost by a factor of two. To interpret this result, the visitor trend of Oktoberfest was investigated. This trend is based on the officially estimated numbers of visitors (muenchen.de (2018)) and was linearly interpolated (see Figure 10). Besides the daily trend, it also shows the mean values of the week- and weekend days (dotted lines). As the number of visitors at Oktoberfest was significantly higher on a weekend day (≈ 1.4) than on a weekday (≈ 0.75) (cf. Figure 10), a higher number of visitors results in higher emission, which indicates the CH_4 emissions are anthropogenic.

3.3   Daily emission cycle

To assess the daily cycle of the CH_4 emissions, the emission numbers of the plume signals $E_{\text{Okt,i,k}}$ are grouped into hourly bins. Then, for each bin an average emission number $E_{\text{Okt,hour,k}}$ is calculated. Afterwards, these numbers are averaged for the 1,000 realizations to obtain robust results including an uncertainty estimate:

$$\mu_{\text{Okt, hour}} = \frac{1}{1000} \sum\nolimits_{k=1}^{1000} E_{\text{Okt, hour},k}, \tag{11}$$

$$\sigma_{\text{Okt,hour}} = \sqrt{\frac{\sum_{k=1}^{1000} (E_{\text{Okt,hour,k}} - \mu_{\text{Okt,hour}}.)^2}{999}} \tag{12}$$
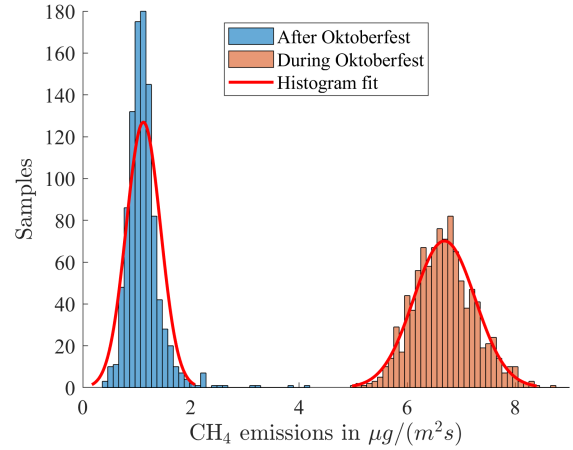
Figure 8. Total CH_4 emission estimates during (light red) and after (blue) the Oktoberfest 2018 including a fitted normal distribution (red line).
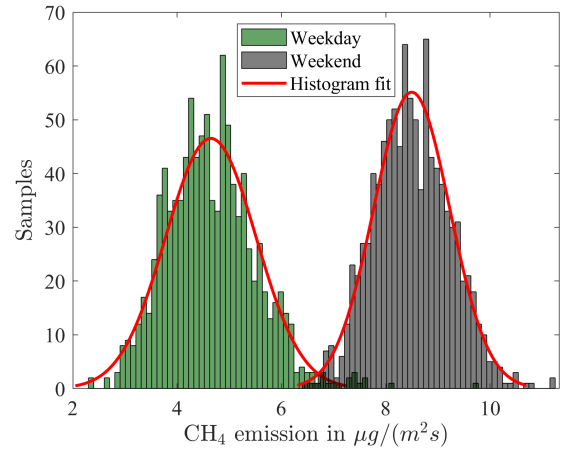
Figure 9. CH_4 emission estimates for a weekday (green) and a weekend day (black) including a fitted normal distribution (red line).

In Figure 11, the variation of the hourly emission mean ($\mu_{\text{Okt, hour}}$) is shown as a blue line. The grey shaded area shows the uncertainty ($\sigma_{\text{Okt,hour}}$) of the emission numbers within that hour. The daily emission cycle shows an oscillating behavior overlaid on an increasing trend towards the evening.

The linear increasing trend is in agreement with Figure 10, which shows a linearly increasing visitor amount throughout the day, confirming the anthropogenic nature of the emissions. The oscillating behavior indicates that the emissions are related to time-dependent events, such as cooking, heating and cleaning, which tends to have the peaks in the morning, noon and evening.
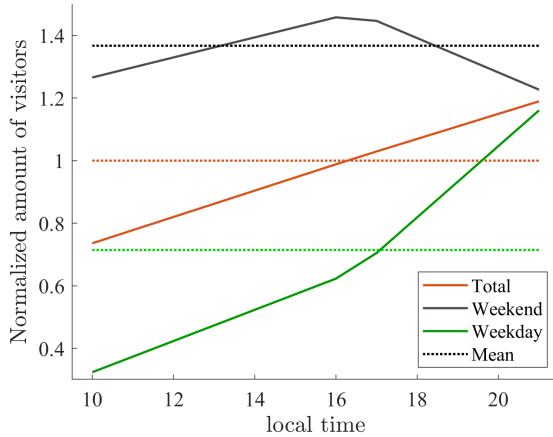
Figure 10. Qualitative daily trend of the number of visitors at Oktoberfest for the weekend (black), weekday (green), and total (red). The dotted line represents the mean value of each trend line.
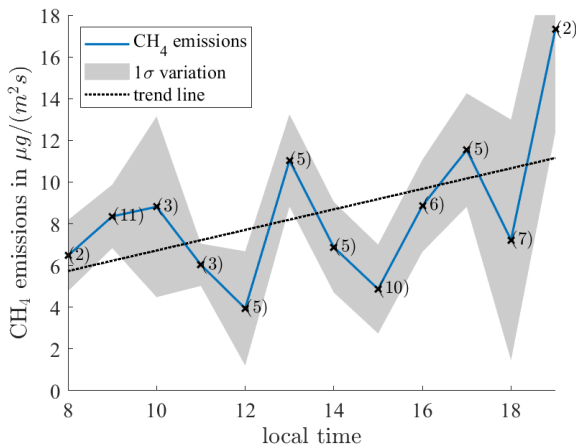
Figure 11. Daily variations of the emissions from the Oktoberfest between 8:00 a.m. and 7:00 p.m. The grey shaded area denotes the variation (1 σ standard deviation) within that hour. The numbers in parentheses indicate the number of valid plumes during that hour.

3.4 Biogenic human CH$_4$ emissions

To address the question whether the people themselves caused the emissions or whether the emissions were caused by processes related to the number of visitors, such as cooking, heating, sewage, etc., we took a closer look at human biogenic emissions.

Most of the previous studies define a methane producer as a person that has a breath CH$_4$ mixing ratio at least 1 ppm above ambient air (Polag and Keppler (2019)). Keppler et al. (2016), however, used laser absorption spectroscopy to confirm that all humans exhale CH$_4$. In that study, the mean of the breath CH$_4$ enhancements above the background from 112 test persons between 1 and 80 years is 2316 ppb and the values vary from 26 ppb to 40.9 ppm.

In addition, we have considered the values reported in Polag and Keppler (2019). The authors provided a summary of various studies of human CH$_4$ emissions in Table 1 and section 3.2, and used these results to calculate average human CH$_4$ emissions, which are 2.3 mmol/d via breath and 7 mmol/d via flatus. We multiplied these values with the 300,000 persons that visit the Oktoberfest premises ($\approx 3.45 \cdot 10^5 \, \mathrm{m}^2$) every day. This represents an upper limit of people who are at the Oktoberfest at the same time, as most visitors do not stay all day long. Please note the average emission numbers are not factor weighted by ethnicity, age and sex, because we do not have those statistics for Oktoberfest. The expected CH$_4$ emission from the human breath and flatulence in total was calculated as:

$$E_{\mathrm{human}} = \frac{(2.3\,\mathrm{mmol/d} + 7\,\mathrm{mmol/d}) \cdot 3 \cdot 10^5}{24\,\mathrm{h} \cdot 3600\,\mathrm{s} \cdot 3.45 \cdot 10^5\,\mathrm{m}^2} = 1.5\,\frac{\mu\mathrm{g}}{\mathrm{m}^2\mathrm{s}}. \tag{13}$$

Although we assumed the maximum possible number of visitors, the resulting biogenic component is 22% of the emissions we determined for Oktoberfest. Therefore, the emissions are not solely produced by the humans themselves, but by processes that are related to the visitor number.

3.5 Emissions from sewage

Besides the direct biogenic human emissions, CH$_4$ emissions from sewer systems are also possible sources. These emissions are a product of bacterial metabolism within waste water, whose emission strength depends particularly on the hydraulic retention time (Liu et al. (2015); Guisasola et al. (2008)) which represents the time the waste water stays in the system. This time decreases with a higher amount of waste water, as the flow increases in such a case.

At Oktoberfest, the amount of waste water is very high as the 100-million liters of water consumed and the 8-million liters of beer have to flow into the sewer system at some time (München (2018b)). Therefore, the retention time in the sewer system underneath the Theresienwiese is quite low, which makes high CH$_4$ emissions from sewage unlikely. Furthermore, the waste water consists mainly of dirty water and

urine, which does not contain many carbon compounds that are necessary to produce CH_4.

3.6   Fossil fuel CH_4 emissions

The biogenic emissions can likely not fully explain the determined emissions of Oktoberfest. Therefore, fossil-fuel related emissions have to be considered as well. According to the weekday/weekend emission comparison (cf. Figure 9) and the daily emission cycle (cf. Figure 11 compared with Figure 10), there is, in general, a visitor-dependent linear increase of CH_4 emissions throughout the day that is superimposed with time-dependent events such as cooking, cleaning or heating. These events can cause CH_4 emissions, as about 40 % of the energy used at Oktoberfest is provided by natural gas used for cooking (79 %) and heating (21 %).

As the human biogenic CH_4 emissions have already been excluded due to too small values, leakages and incomplete burning in the gas appliances provide a possibility to explain the emissions. C_2H_6 is a tracer of thermogenic CH_4, and therefore can be used to indicate a natural gas related source (Yacovitch et al. (2014); McKain et al. (2015)). For that reason, we deployed a portable instrument designed to measure CH_4 but that is also capable of measuring C_2H_6. Due to the aforementioned safety reasons, the distance between the measurements and the closest point source (tent) was $50\,\mathrm{m}$ to $250\,\mathrm{m}$. Therefore, the CH_4 concentration was relatively low (max. 100 ppb). According to the Munich municipal utilities, the C_2H_6/CH_4 ratio of natural gas used in Munich is about 3 % (München (2018c)), which results in an C_2H_6 concentration lower than 3 ppb, assuming that all of the measured CH_4 is sourced from natural gas. Such a small concentration value is lower than the detection limit of the GasScouter (about $3\,\mathrm{ppb}$ with $10\,\mathrm{s}$ integration time), which is why we were not able to determine the C_2H_6/CH_4 ratio of the measured gas.

Nevertheless, it is possible to determine an upper bound for the loss rate of natural gas if one assumes that all the emissions are fossil-fuel based. The natural gas consumption at Oktoberfest 2018 added up to $200{,}937\,\mathrm{m}^3$. Therefore, the total weight of the consumed CH_4 at Oktoberfest yields

$$M_{\mathrm{gas,total}} = 0.668\,\mathrm{kg\,m^{-3}} \cdot 200{,}937\,\mathrm{m}^3 = 1.34 \cdot 10^5\,\mathrm{kg}. \quad (14)$$

In this study, the CH_4 flux of Oktoberfest has been determined to be $6.7\,\mathrm{\mu g/(m^2 s)}$. If we assume that the emission is continuous throughout the day (about $11\,\mathrm{h}$ opening time per day) and homogeneous throughout the entire Oktoberfest premises, the total amount of CH_4 lost to the atmosphere would be:

$$M_{\mathrm{CH4,loss,max}} = 6.7\,\frac{\mathrm{\mu g}}{\mathrm{m^2 s}} \cdot \left(16\,\mathrm{d} \cdot 11\,\frac{\mathrm{h}}{\mathrm{d}} \cdot 3600\,\frac{\mathrm{s}}{\mathrm{h}}\right) \cdot 3.45 \cdot 10^5\,\mathrm{m}^2$$
$$= 1.46 \cdot 10^3\,\mathrm{kg}. \quad (15)$$

The CH_4 share of the natural gas in Munich is on average about 96 % (München (2018c)). If we assume all of the CH_4

Table 2. Comparison of the Oktoberfest emission flux to state-of-the-art emission inventory fluxes for the same location.

Description	Year	Flux	Averaging area
Oktoberfest	2018	$6.7\,\mathrm{\mu g/(m^2 s)}$	$0.3\,\mathrm{km}^2$
TNO-MACC III	2015	$0.9\,\mathrm{\mu g/(m^2 s)}$	$4.6\,\mathrm{km}^2$
EDGAR v4.3.2	2012	$1.0\,\mathrm{\mu g/(m^2 s)}$	$82\,\mathrm{km}^2$
IER	2008	$0.1\,\mathrm{\mu g/(m^2 s)}$	$4.0\,\mathrm{km}^2$

emissions are fossil-fuel related, the maximum loss rate can be determined as:

$$\frac{M_{\mathrm{CH4,loss,max}}}{M_{\mathrm{CH4,total}}} = \frac{1.46 \cdot 10^3\,\mathrm{kg}}{1.34 \cdot 10^5\,\mathrm{kg} \cdot 96\%} = 1.1\,\%. \quad (16)$$

This loss rate of 1.1 % is smaller than the gas leaks reported in the literature, such as a 2.7 % loss rate for the urban region of Boston (McKain et al. (2015)) or 2.3 % for the U.S. oil and gas supply chain (Alvarez et al. (2018)).

3.7   Comparison with existing CH_4 emission estimates

To the best of our knowledge, there is no comparable CH_4 study dealing with festivals. For a better illustration, we compared the emission flux of the Oktoberfest premises to the emission flux of Boston, which is known as a very leaky city. In the Boston study, McKain et al. (2015) quantified the regional averaged emission flux of CH_4 there as $(18.5 \pm 3.7)\,\mathrm{g/(m^2 a)}$ (95 % confidence interval), which corresponds to $(0.6 \pm 0.1)\,\mathrm{\mu g/(m^2 s)}$ and is less than a tenth of the emissions that we determined for the Oktoberfest premises. Although it is difficult to compare the small and densely populated Oktoberfest premises with the entire city area of Boston, the comparison shows that the emission flux of Oktoberfest is significant.

Furthermore, we compared the Oktoberfest emission flux to the state-of-the-art emission inventory fluxes of that quarter of Munich. For that purpose, the annual emission fluxes of TNO-MACC III (2015) (Denier van der Gon et al. (2017); Kuenen et al. (2014)), EDGAR v4.3.2 (2012) (Janssens-Maenhout et al. (2019)) and IER (2008) (Pregger et al.) are converted to the common unit $\mathrm{\mu g/(m^2 s)}$. In Table 2, the converted values are shown. Furthermore, one can see that the different inventories have different spatial resolutions. Therefore, the fluxes are averaged over areas that represent not only the Oktoberfest premises but also additional urban districts. Nevertheless, the Oktoberfest emissions are significantly higher than all three inventories considered. Therefore, festivals such as Oktoberfest can be significant CH_4 sources. Although only present for a limited time each year, they should be included in the inventories.

4 Conclusions and Outlook

This is the first study that deals with the methane emissions of a big festival. We investigated Oktoberfest as it is the world's largest folk festival and a methane source that had not yet been taken into account in the emission inventories.

Combining the in-situ measurements with a Gaussian plume dispersion model, the average emission of Oktoberfest was determined to be $(6.7 \pm 0.6)\,\mu g/(m^2 s)$ ($1\,\sigma$ standard deviation). A comparison between weekdays $(4.6\,\mu g/(m^2 s))$ and weekend days $(8.5\,\mu g/(m^2 s))$ shows that the emission strength at the weekend was almost twice as high compared to during the week. It demonstrates that a higher number of visitors results in higher emissions. However, the daily emission cycle has an oscillating behavior that cannot be explained by the number of visitors. These results suggest that CH_4 emissions at Oktoberfest do not come solely from the human biogenic emissions, which was 5 times smaller than the emissions determined for the Oktoberfest according to our calculations. Fossil-fuel related emissions, such as incomplete combustion or loss in the gas appliances, are more likely the major contributors to Oktoberfest emissions.

Due to safety reasons, we were not allowed to enter the festival premises with the instrument. Therefore, the distance from the measurement points to the suspected sources on the festival terrain was large, which resulted in low CH_4 and C_2H_6 concentrations. The latter ones were even below the detection limit of the instrument. This limited the possibilities to attribute the emissions to specific sources. To improve this aspect, several additional approaches are possible for future studies. As we are not aware of a more sensitive portable C_2H_6 analyzer, discrete air sampling using sample bags within the tents for C_2H_6 is an option. Furthermore, the measurement of isotope ratios, such as $\delta 13C$ and δD, are useful options to improve the source attribution. For other festivals, researchers might be allowed to get closer to the sources.

The method introduced in this paper is comparatively straightforward; it can be applied widely to discover and quantify overlapping methane sources: groups of small cow barns, uncovered heaps in landfills, or wetlands made of groups of ponds and swamps, etc.

In summary, this study uses Oktoberfest as an exemplary event to show, for the first time, that large festivals can be significant CH_4 emitters. Therefore, these events should be included in future emission inventories. Furthermore, our results provide the foundation to develop reduction policies for such events and a new pathway to mitigate fossil fuel CH_4 emissions.

Data availability. All raw data can be provided by the corresponding authors upon request.

Author contributions. JC, FD and HM planned the campaign; JC, FD, HM, AF and DW performed the measurements; JC, FD, AF and DW analyzed the data; JC and FD wrote the manuscript draft; AF, MH, HDG and TR reviewed and edited the manuscript.

Competing interests. The authors declare that they have no conflict of interest.

Acknowledgements. We thank Peter Swinkels and his colleagues from Picarro Inc. who made it possible for us to borrow the GasScouter; Jörg Ochs (Munich municipal utilities, SWM) for providing us helpful information about the Munich gas distribution system; Hanns-Erik Endres, Manfred Engl and colleagues from Fraunhofer EMFT, Martin Christ (LMU) as well as the colleagues from Klenze Gymnasium Munich for providing access to measurement sites; Markus Garhammer, Matthias Wiegner and Mark Wenig (LMU) for providing us wind and boundary layer height data; Anna-Leah Nickl and Mariano Mertens (DLR) for running high-resolution wind forecasts; Konrad Koch (TUM) for providing us detailed information about the Munich sewer system; Rachel Chang for fruitful discussions; our students Ankit Shekhar, Xiao Bi and Homa Ghasemifard for helping with the measurements; Stephen Starck, Ankit Shekhar, and Rita von Grafenstein for proofreading the paper. We acknowledge the financial support from Technische Universität München – Institute for Advanced Study, funded by the German Excellence Initiative and the European Union Seventh Framework Programme under grant agreement no. 291763.

References

Allen, M. R., Shine, K. P., Fuglestvedt, J. S., Millar, R. J., Cain, M., Frame, D. J., and Macey, A. H.: A solution to the misrepresentations of CO 2 -equivalent emissions of short-lived climate pollutants under ambitious mitigation, npj Climate and Atmospheric Science, 1, 16, https://doi.org/10.1038/s41612-018-0026-8, https://www.nature.com/articles/s41612-018-0026-8, 2018.

Alvarez, R. A., Zavala-Araiza, D., Lyon, D. R., Allen, D. T., Barkley, Z. R., Brandt, A. R., Davis, K. J., Herndon, S. C., Jacob, D. J., Karion, A., Kort, E. A., Lamb, B. K., Lauvaux, T., Maasakkers, J. D., Marchese, A. J., Omara, M., Pacala, S. W., Peischl, J., Robinson, A. L., Shepson, P. B., Sweeney, C., Townsend-Small, A., Wofsy, S. C., and Hamburg, S. P.: Assessment of methane emissions from the U.S. oil and gas supply chain, Science, 361, 186–188, https://doi.org/10.1126/science.aar7204, https://science.sciencemag.org/content/361/6398/186, 2018.

Atherton, E., Risk, D., Fougère, C., Lavoie, M., Marshall, A., Werring, J., Williams, J. P., and Minions, C.: Mobile measurement of methane emissions from natural gas developments in northeastern British Columbia, Canada, Atmospheric Chemistry and Physics, 17, 12 405–12 420, https://doi.org/https://doi.org/10.5194/acp-17-12405-2017, https://www.atmos-chem-phys.net/17/12405/2017/, 2017.

Bovensmann, H., Buchwitz, M., Burrows, J. P., Reuter, M., Krings, T., Gerilowski, K., Schneising, O., Heymann, J., Tretner, A., and Erzinger, J.: A remote sensing technique for global mon-

itoring of power plant CO_2 emissions from space and related applications, Atmospheric Measurement Techniques, 3, 781–811, https://doi.org/10.5194/amt-3-781-2010, http://www.atmos-meas-tech.net/3/781/2010/, 2010.

Briggs, G. A.: Diffusion estimation for small emissions. Preliminary report, Tech. Rep. TID-28289, National Oceanic and Atmospheric Administration, Oak Ridge, Tenn. (USA). Atmospheric Turbulence and Diffusion Lab., https://doi.org/10.2172/5118833, https://www.osti.gov/biblio/5118833-diffusion-estimation-small-emissions-preliminary-report, 1973.

Chen, J., Viatte, C., Hedelius, J. K., Jones, T., Franklin, J. E., Parker, H., Gottlieb, E. W., Wennberg, P. O., Dubey, M. K., and Wofsy, S. C.: Differential column measurements using compact solar-tracking spectrometers, Atmospheric Chemistry and Physics, 16, 8479–8498, https://doi.org/10.5194/acp-16-8479-2016, https://www.atmos-chem-phys.net/16/8479/2016/, 2016.

Chen, J., Dietrich, F., Franklin, J., Jones, T., Butz, A., Luther, A., Kleinschek, R., Hase, F., Wenig, M., Ye, S., Nouri, A., Frey, M., Knote, C., Alberti, C., and Wofsy, S.: Mesoscale Column Network for Assessing GHG and NOx Emissions in Munich, in: Geophysical Research Abstracts, vol. 20, pp. EGU2018–10 192–2, 2018.

Denier van der Gon, H. A. C., Kuenen, J. J. P., Janssens-Maenhout, G., Döring, U., Jonkers, S., and Visschedijk, A.: TNO_CAMS high resolution European emission inventory 2000–2014 for anthropogenic CO_2 and future years following two different pathways, Earth System Science Data Discussions, pp. 1–30, https://doi.org/https://doi.org/10.5194/essd-2017-124, https://www.earth-syst-sci-data-discuss.net/essd-2017-124/, 2017.

Etminan, M., Myhre, G., Highwood, E. J., and Shine, K. P.: Radiative forcing of carbon dioxide, methane, and nitrous oxide: A significant revision of the methane radiative forcing, Geophysical Research Letters, 43, 12,614–12,623, https://doi.org/10.1002/2016GL071930, https://agupubs.onlinelibrary.wiley.com/doi/abs/10.1002/2016GL071930, 2016.

Gifford, F. A.: Turbulent diffusion-typing schemes: a review, http://inis.iaea.org/Search/search.aspx?orig_q=RN:8296495, 1976.

Guisasola, A., de Haas, D., Keller, J., and Yuan, Z.: Methane formation in sewer systems, Water Research, 42, 1421–1430, https://doi.org/10.1016/j.watres.2007.10.014, http://www.sciencedirect.com/science/article/pii/S0043135407006483, 2008.

Hanna, S. R., Briggs, G. A., and Hosker, R. P. J.: Handbook on atmospheric diffusion, Tech. Rep. DOE/TIC-11223, National Oceanic and Atmospheric Administration, Oak Ridge, TN (USA). Atmospheric Turbulence and Diffusion Lab., https://doi.org/10.2172/5591108, https://www.osti.gov/biblio/5591108-handbook-atmospheric-diffusion, 1982.

Hausmann, P., Sussmann, R., and Smale, D.: Contribution of oil and natural gas production to renewed increase in atmospheric methane (2007–2014): top–down estimate from ethane and methane column observations, Atmospheric Chemistry and Physics, 16, 3227–3244, https://doi.org/https://doi.org/10.5194/acp-16-3227-2016, https://www.atmos-chem-phys.net/16/3227/2016/, 2016.

Huang, K., Zhuang, G., Lin, Y., Wang, Q., Fu, J. S., Zhang, R., Li, J., Deng, C., and Fu, Q.: Impact of anthropogenic emission on air quality over a megacity – revealed from an intensive atmospheric campaign during the Chinese Spring Festival, Atmospheric Chemistry and Physics, 12, 11 631–11 645, https://doi.org/https://doi.org/10.5194/acp-12-11631-2012, https://www.atmos-chem-phys.net/12/11631/2012/, 2012.

IPCC: IPCC Climate Change 2013: The Physical Science Basis. Contribution of Working Group I to the Fourth Assessment Report of the Intergovernmental Panel on Climate Change, p. 1535, Cambridge University Press, Cambridge, 2013.

Janssens-Maenhout, G., Crippa, M., Guizzardi, D., Muntean, M., Schaaf, E., Dentener, F., Bergamaschi, P., Pagliari, V., Olivier, J. G. J., Peters, J. A. H. W., Aardenne, J. A. v., Monni, S., Doering, U., Petrescu, A. M. R., Solazzo, E., and Oreggioni, G. D.: EDGAR v4.3.2 Global Atlas of the three major greenhouse gas emissions for the period 1970–2012, Earth System Science Data, 11, 959–1002, https://doi.org/https://doi.org/10.5194/essd-11-959-2019, https://www.earth-syst-sci-data.net/11/959/2019/essd-11-959-2019-discussion.html, 2019.

Kaiser, J. and Schafer, R.: On the use of the I0-sinh window for spectrum analysis, IEEE Transactions on Acoustics, Speech, and Signal Processing, 28, 105–107, https://doi.org/10.1109/TASSP.1980.1163349, 1980.

Keppler, F., Schiller, A., Ehehalt, R., Greule, M., Hartmann, J., and Polag, D.: Stable isotope and high precision concentration measurements confirm that all humans produce and exhale methane, J Breath Res, 10, 016 003, https://doi.org/10.1088/1752-7155/10/1/016003, 2016.

Kiemle, C., Ehret, G., Amediek, A., Fix, A., Quatrevalet, M., and Wirth, M.: Potential of Spaceborne Lidar Measurements of Carbon Dioxide and Methane Emissions from Strong Point Sources, Remote Sensing, 9, 1137, https://doi.org/10.3390/rs9111137, https://www.mdpi.com/2072-4292/9/11/1137, 2017.

Kirschke, S., Bousquet, P., Ciais, P., Saunois, M., Canadell, J. G., Dlugokencky, E. J., Bergamaschi, P., Bergmann, D., Blake, D. R., Bruhwiler, L., Cameron-Smith, P., Castaldi, S., Chevallier, F., Feng, L., Fraser, A., Heimann, M., Hodson, E. L., Houweling, S., Josse, B., Fraser, P. J., Krummel, P. B., Lamarque, J.-F., Langenfelds, R. L., Le Quéré, C., Naik, V., O'Doherty, S., Palmer, P. I., Pison, I., Plummer, D., Poulter, B., Prinn, R. G., Rigby, M., Ringeval, B., Santini, M., Schmidt, M., Shindell, D. T., Simpson, I. J., Spahni, R., Steele, L. P., Strode, S. A., Sudo, K., Szopa, S., van der Werf, G. R., Voulgarakis, A., van Weele, M., Weiss, R. F., Williams, J. E., and Zeng, G.: Three decades of global methane sources and sinks, Nature Geoscience, 6, 813–823, https://doi.org/10.1038/ngeo1955, https://www.nature.com/articles/ngeo1955, 2013.

Kuenen, J. J. P., Visschedijk, A. J. H., Jozwicka, M., and Denier van der Gon, H. a. C.: TNO-MACC_II emission inventory; a multi-year (2003–2009) consistent high-resolution European emission inventory for air quality modelling, Atmospheric Chemistry and Physics, 14, 10 963–10 976, https://doi.org/https://doi.org/10.5194/acp-14-10963-2014, https://www.atmos-chem-phys.net/14/10963/2014/, 2014.

Kuo, C.-Y., Lee, H.-S., and Lai, J.-H.: Emission of polycyclic aromatic hydrocarbons and lead during Chinese mid-autumn festival, Sci. Total Environ., 366, 233–241, https://doi.org/10.1016/j.scitotenv.2005.08.006, 2006.

Lamb, B. K., Cambaliza, M. O. L., Davis, K. J., Edburg, S. L., Ferrara, T. W., Floerchinger, C., Heimburger, A. M. F., Herndon, S., Lauvaux, T., Lavoie, T., Lyon, D. R., Miles, N., Prasad,

K. R., Richardson, S., Roscioli, J. R., Salmon, O. E., Shepson, P. B., Stirm, B. H., and Whetstone, J.: Direct and Indirect Measurements and Modeling of Methane Emissions in Indianapolis, Indiana, Environ. Sci. Technol., 50, 8910–8917, https://doi.org/10.1021/acs.est.6b01198, https://doi.org/10.1021/acs.est.6b01198, 2016.

Liu, Y., Ni, B.-J., Sharma, K. R., and Yuan, Z.: Methane emission from sewers, Science of The Total Environment, 524-525, 40–51, https://doi.org/10.1016/j.scitotenv.2015.04.029, http://www.sciencedirect.com/science/article/pii/S0048969715004659, 2015.

Luther, A., Kleinschek, R., Scheidweiler, L., Defratyka, S., Stanisavljevic, M., Forstmaier, A., Dandocsi, A., Wolff, S., Dubravica, D., Wildmann, N., Kostinek, J., Jöckel, P., Nickl, A.-L., Klausner, T., Hase, F., Frey, M., Chen, J., Dietrich, F., Nęcki, J., Swolkień, J., Fix, A., Roiger, A., and Butz, A.: Towards verifying CH_4 emissions from hard coal mines using mobile sun-viewing Fourier transform spectrometry, Atmospheric Measurement Techniques Discussions, pp. 1–19, https://doi.org/https://doi.org/10.5194/amt-2019-205, https://www.atmos-meas-tech-discuss.net/amt-2019-205/, 2019.

McKain, K., Down, A., Raciti, S. M., Budney, J., Hutyra, L. R., Floerchinger, C., Herndon, S. C., Nehrkorn, T., Zahniser, M. S., Jackson, R. B., and others: Methane emissions from natural gas infrastructure and use in the urban region of Boston, Massachusetts, Proceedings of the National Academy of Sciences, 112, 1941–1946, 2015.

muenchen.de: Oktoberfest-Barometer: Die beste Zeit für den Wiesnbesuch, https://www.muenchen.de/veranstaltungen/oktoberfest/besucher-service/wiesnbarometer.html, 2018.

Myhre, G., Samset, B. H., Schulz, M., Balkanski, Y., Bauer, S., Berntsen, T. K., Bian, H., Bellouin, N., Chin, M., Diehl, T., Easter, R. C., Feichter, J., Ghan, S. J., Hauglustaine, D., Iversen, T., Kinne, S., Kirkevåg, A., Lamarque, J.-F., Lin, G., Liu, X., Lund, M. T., Luo, G., Ma, X., Noije, T. v., Penner, J. E., Rasch, P. J., Ruiz, A., Seland, Ø., Skeie, R. B., Stier, P., Takemura, T., Tsigaridis, K., Wang, P., Wang, Z., Xu, L., Yu, H., Yu, F., Yoon, J.-H., Zhang, K., Zhang, H., and Zhou, C.: Radiative forcing of the direct aerosol effect from AeroCom Phase II simulations, Atmospheric Chemistry and Physics, 13, 1853–1877, https://doi.org/https://doi.org/10.5194/acp-13-1853-2013, https://www.atmos-chem-phys.net/13/1853/2013/, 2013.

München, S.: Oktoberfest 2018 Schlussbericht, https://www.ris-muenchen.de/RII/RII/DOK/SITZUNGSVORLAGE/5440803.pdf, 2018a.

München, S.: Oktoberfest 2018 Schlussbericht, https://www.ris-muenchen.de/RII/RII/DOK/SITZUNGSVORLAGE/5440803.pdf, 2018b.

München, S.: Erdgasbeschaffenheit: Jahresmittel für 2018, https://www.swm-infrastruktur-region.de/dam/swm-infrastruktur-region/dokumente/erdgas/netzstrukturdaten/erdgasbeschaffenheit-jahresmittel-2018.pdf, 2018c.

Nassar, R., Hill, T. G., McLinden, C. A., Wunch, D., Jones, D. B. A., and Crisp, D.: Quantifying CO2 Emissions From Individual Power Plants From Space, Geophysical Research Letters, 44, 10,045–10,053, https://doi.org/10.1002/2017GL074702, https://agupubs.onlinelibrary.wiley.com/doi/abs/10.1002/2017GL074702, 2017.

Nisbet, E. G., Dlugokencky, E. J., and Bousquet, P.: Methane on the Rise—Again, Science, 343, 493–495, https://doi.org/10.1126/science.1247828, https://science.sciencemag.org/content/343/6170/493, 2014.

Nishanth, T., Praseed, K. M., Rathnakaran, K., Satheesh Kumar, M. K., Ravi Krishna, R., and Valsaraj, K. T.: Atmospheric pollution in a semi-urban, coastal region in India following festival seasons, Atmospheric Environment, 47, 295–306, https://doi.org/10.1016/j.atmosenv.2011.10.062, http://www.sciencedirect.com/science/article/pii/S1352231011011551, 2012.

O'Keefe, A. and Deacon, D. A. G.: Cavity ring-down optical spectrometer for absorption measurements using pulsed laser sources, Review of Scientific Instruments, 59, 2544–2551, https://doi.org/10.1063/1.1139895, https://aip.scitation.org/doi/10.1063/1.1139895, 1988.

Pasquill, F.: Lagrangian similarity and vertical diffusion from a source at ground level, Quarterly Journal of the Royal Meteorological Society, 92, 185–195, https://doi.org/10.1002/qj.49709239202, https://rmets.onlinelibrary.wiley.com/doi/abs/10.1002/qj.49709239202, 1966.

Pasquill, F.: The Influence of the Turning of Wind with Height on Crosswind Diffusion, Philosophical Transactions of the Royal Society of London. Series A, Mathematical and Physical Sciences, 265, 173–181, https://www.jstor.org/stable/73723, 1969.

Pasquill, F.: Atmospheric Dispersion Modeling, Journal of the Air Pollution Control Association, 29, 117–119, https://doi.org/10.1080/00022470.1979.10470764, http://www.tandfonline.com/doi/abs/10.1080/00022470.1979.10470764, 1979.

Phillips, N. G., Ackley, R., Crosson, E. R., Down, A., Hutyra, L. R., Brondfield, M., Karr, J. D., Zhao, K., and Jackson, R. B.: Mapping urban pipeline leaks: Methane leaks across Boston, Environmental Pollution, 173, 1–4, https://doi.org/10.1016/j.envpol.2012.11.003, http://www.sciencedirect.com/science/article/pii/S0269749112004800, 2013.

Picarro: Datasheet GasScouter G4302 CH_4, C_2H_6 and H_2O Analyzer, https://www.picarro.com/support/library/documents/gasscoutertm_g4302_analyzer_data_sheet, 2017.

Plant, G., Kort, E. A., Floerchinger, C., Gvakharia, A., Vimont, I., and Sweeney, C.: Large Fugitive Methane Emissions From Urban Centers Along the U.S. East Coast, https://doi.org/10.1029/2019GL082635, https://agupubs.onlinelibrary.wiley.com/doi/abs/10.1029/2019GL082635, 2019.

Polag, D. and Keppler, F.: Global methane emissions from the human body: Past, present and future, Atmospheric Environment, 214, 116 823, https://doi.org/10.1016/j.atmosenv.2019.116823, http://www.sciencedirect.com/science/article/pii/S1352231019304522, 2019.

Pregger, T., Scholz, Y., and Friedrich, R.: Documentation of the Anthropogenic GHG Emission Data for Europe Provided in the Frame of CarboEurope GHG and CarboEurope IP, p. 41.

Roscioli, J. R., Yacovitch, T. I., Floerchinger, C., Mitchell, A. L., Tkacik, D. S., Subramanian, R., Martinez, D. M., Vaughn, T. L., Williams, L., Zimmerle, D., Robinson, A. L., Herndon, S. C., and Marchese, A. J.: Measurements of methane emissions from natural gas gathering facilities and processing plants:

measurement methods, Atmospheric Measurement Techniques, 8, 2017–2035, https://doi.org/https://doi.org/10.5194/amt-8-2017-2015, https://www.atmos-meas-tech.net/8/2017/2015/amt-8-2017-2015.html, 2015.

Saunois, M., Jackson, R. B., Bousquet, P., Poulter, B., and Canadell, J. G.: The growing role of methane in anthropogenic climate change, Environ. Res. Lett., 11, 120 207, https://doi.org/10.1088/1748-9326/11/12/120207, https://doi.org/10.1088%2F1748-9326%2F11%2F12%2F120207, 2016.

Schwietzke, S., Griffin, W. M., Matthews, H. S., and Bruhwiler, L. M. P.: Natural Gas Fugitive Emissions Rates Constrained by Global Atmospheric Methane and Ethane, Environ. Sci. Technol., 48, 7714–7722, https://doi.org/10.1021/es501204c, https://doi.org/10.1021/es501204c, 2014.

Schwietzke, S., Sherwood, O. A., Bruhwiler, L. M. P., Miller, J. B., Etiope, G., Dlugokencky, E. J., Michel, S. E., Arling, V. A., Vaughn, B. H., White, J. W. C., and Tans, P. P.: Upward revision of global fossil fuel methane emissions based on isotope database, Nature, 538, 88–91, https://doi.org/10.1038/nature19797, https://www.nature.com/articles/nature19797, 2016.

Shi, G.-L., Liu, G.-R., Tian, Y.-Z., Zhou, X.-Y., Peng, X., and Feng, Y.-C.: Chemical characteristic and toxicity assessment of particle associated PAHs for the short-term anthropogenic activity event: During the Chinese New Year's Festival in 2013, Sci. Total Environ., 482-483, 8–14, https://doi.org/10.1016/j.scitotenv.2014.02.107, 2014.

Toja-Silva, F., Chen, J., Hachinger, S., and Hase, F.: CFD simulation of CO_2 dispersion from urban thermal power plant: Analysis of turbulent Schmidt number and comparison with Gaussian plume model and measurements, Journal of Wind Engineering and Industrial Aerodynamics, 169, 177–193, https://doi.org/10.1016/j.jweia.2017.07.015, http://www.sciencedirect.com/science/article/pii/S0167610517302258, 2017.

von Fischer, J. C., Cooley, D., Chamberlain, S., Gaylord, A., Griebenow, C. J., Hamburg, S. P., Salo, J., Schumacher, R., Theobald, D., and Ham, J.: Rapid, Vehicle-Based Identification of Location and Magnitude of Urban Natural Gas Pipeline Leaks, Environ. Sci. Technol., 51, 4091–4099, https://doi.org/10.1021/acs.est.6b06095, https://doi.org/10.1021/acs.est.6b06095, 2017.

Weller, Z. D., Roscioli, J. R., Daube, W. C., Lamb, B. K., Ferrara, T. W., Brewer, P. E., and von Fischer, J. C.: Vehicle-Based Methane Surveys for Finding Natural Gas Leaks and Estimating Their Size: Validation and Uncertainty, Environ. Sci. Technol., 52, 11 922–11 930, https://doi.org/10.1021/acs.est.8b03135, https://doi.org/10.1021/acs.est.8b03135, 2018.

Worden, J. R., Bloom, A. A., Pandey, S., Jiang, Z., Worden, H. M., Walker, T. W., Houweling, S., and Röckmann, T.: Reduced biomass burning emissions reconcile conflicting estimates of the post-2006 atmospheric methane budget, Nature Communications, 8, 2227, https://doi.org/10.1038/s41467-017-02246-0, https://www.nature.com/articles/s41467-017-02246-0, 2017.

Wunch, D., Toon, G. C., Hedelius, J. K., Vizenor, N., Roehl, C. M., Saad, K. M., Blavier, J.-F. L., Blake, D. R., and Wennberg, P. O.: Quantifying the loss of processed natural gas within California's South Coast Air Basin using long-term measurements

of ethane and methane, Atmospheric Chemistry and Physics, 16, 14 091–14 105, https://doi.org/10.5194/acp-16-14091-2016, https://www.atmos-chem-phys.net/16/14091/2016/, 2016.

Yacovitch, T. I., Herndon, S. C., Roscioli, J. R., Floerchinger, C., McGovern, R. M., Agnese, M., Pétron, G., Kofler, J., Sweeney, C., Karion, A., Conley, S. A., Kort, E. A., Nähle, L., Fischer, M., Hildebrandt, L., Koeth, J., McManus, J. B., Nelson, D. D., Zahniser, M. S., and Kolb, C. E.: Demonstration of an ethane spectrometer for methane source identification, Environ. Sci. Technol., 48, 8028–8034, https://doi.org/10.1021/es501475q, 2014.

Yacovitch, T. I., Herndon, S. C., Pétron, G., Kofler, J., Lyon, D., Zahniser, M. S., and Kolb, C. E.: Mobile Laboratory Observations of Methane Emissions in the Barnett Shale Region, Environ. Sci. Technol., 49, 7889–7895, https://doi.org/10.1021/es506352j, https://doi.org/10.1021/es506352j, 2015.

Yacovitch, T. I., Neininger, B., Herndon, S. C., Gon, H. D. v. d., Jonkers, S., Hulskotte, J., Roscioli, J. R., and Zavala-Araiza, D.: Methane emissions in the Netherlands: The Groningen field, Elem Sci Anth, 6, 57, https://doi.org/10.1525/elementa.308, http://www.elementascience.org/articles/10.1525/elementa.308/, 2018.